Cyclic nanoindentation and Raman microspectroscopy study of phase transformations in semiconductors

Yury G. Gogotsi and Vladislav Domnich
University of Illinois at Chicago, Department of Mechanical Engineering, 842 West Taylor Street, Chicago, Illinois 60607-7022

Sergey N. Dub
Institute for Superhard Materials, 2 Avtozavodskaya St., Kiev 254074, Ukraine

Andreas Kailer[a)] and Klaus G. Nickel
Universität Tübingen, Institut für Mineralogie, Petrologie und Geochemie, Wilhelmstr. 56, D-72074 Tübingen, Germany

(Received 7 December 1998; accepted 1 February 2000)

This paper supplies new interpretation of nanoindentation data for silicon, germanium, and gallium arsenide based on Raman microanalysis of indentations. For the first time, Raman microspectroscopy analysis of semiconductors within nanoindentations is reported. The given analysis of the load-displacement curves shows that depth-sensing indentation can be used as a tool for identification of pressure-induced phase transformations. Volume change upon reverse phase transformation of metallic phases results either in a pop-out (or a kink-back) or in a slope change (elbow) of the unloading part of the load-displacement curve. Broad and asymmetric hysteresis loops of changing width, as well as changing slope of the elastic part of the loading curve in cyclic indentation can be used for confirmation of a phase transformation during indentation. Metallization pressure can be determined as average contact pressure (Meyer's hardness) for the yield point on the loading part of the load-displacement curve. The pressure of the reverse transformation of the metallic phase can be measured from pop-out or elbow on the unloading part of the diagram. For materials with phase transformations less pronounced than in Si, replotting of the load-displacement curves as average contact pressure versus relative indentation depth is required to determine the transformation pressures and/or improve the accuracy of data interpretation.

I. INTRODUCTION

It is known that the indentation of materials creates high stresses (hydrostatic and deviatoric) under diamond indenters that can cause pressure-induced phase transformations.[1–6] It has also been shown that the hardness correlates with metallization pressures for a number of semiconductors.[7] The conditions for phase transformation are complex, involving numerous parameters such as the shape of indenter, maximum load, loading rate, and temperature. Understanding of the mechanism of the processes under sharp indenters is of tremendous importance for interpretation of indentation data.

All previous depth-sensing indentation studies conducted on Si, Ge, and GaAs showed that only silicon displays a characteristic pop-out event on pressure release.[8] Metallization of Si and Ge during nanoindentation has been confirmed from conductivity measurements.[5] Scanning electron microscope (SEM) images of nanoindentations in Si[4] and Ge[8] revealed an extruded layer within the contact area after indentation and provided evidence of similarity of the metallization processes in indentation of Si and Ge.[9] Transmission electron microscope (TEM) studies showed no dislocation activity operating outside the transformation zone within nanoindentations of silicon and revealed amorphous transformation zone under the indentation center with an adjacent region of plastic extruded material.[10] To the best of our knowledge, no studies supporting the metallization or amorphization of GaAs during nanoindentation have been conducted so far.

Our recent work[2,3] demonstrated that Raman microspectroscopy is the most powerful tool to trace phase transformations in indentation area. However, all previous Raman data were obtained on microindentations of typically >5 μm in size. No Raman analysis of nanoin-

[a)]Present address: Fraunhofer-Institut für Werkstoffmechanik (Fh-IWM), Wöhlerstr. 11, D-79108 Freiburg, Germany.

dentations having the size of ≤1 μm has been reported in the literature. In the present work, we compare results of nanoindentation and Raman microspectroscopy studies with the purpose of establishing correlation between phase transformations and nanoindentation data. Signs of phase transformations in the load-displacement and average contact pressure (ACP) versus indentation depth plots obtained in nanoindentation experiments will be discussed.

II. MATERIALS AND EXPERIMENTAL

Nanoindentation experiments were performed using a Nano Indenter II® tester (MTS). The continuously recorded load and displacement provide a material's response to deformation.

Several samples of semiconductors were indented using a Berkovich pyramidal indenter. Semiconductors in the experiments include silicon, germanium, and gallium arsenide single crystals (Table I). The samples were oriented arbitrarily, but as previous work on Si shows, crystal orientation has only a minor effect on nanoindentation data.[8] Cyclic nanoindentation tests were performed by the following way: (i) loading to 10 mN and unloading by 95%, (ii) loading to 20 mN and unloading by 95%, (iii) loading to 30 mN and unloading by 95%, (iv) loading to 40 mN and unloading by 90%, (v) hold for 20 s at 10% of the maximum load for thermal drift correction, and (vi) complete unloading.

The unloading rate was the same as the loading rate. Four different rates from 100 to 3000 μN/s were used in these experiments. It is necessary to note that at very low loading rates (<1000 μN/s) creep during loading can affect the experimental results. The procedure suggested in Ref. 11 was used to monitor the ACP in the indent.

Raman spectra were recorded using LabRam II (Dilor, France) and Ramascope 2000 (Renishaw, UK) Raman microspectrometers equipped with charge-coupled device detectors and microscopes for focusing the incident laser beam to a 1-μm spot. The 514.5-nm (Ar ion laser) and 632.8-nm (He–Ne laser) excitation lines were used. The acquisition time varied from 10 to 300 s depending on the sample and the intensity of the laser beam. In order not to produce artifacts by laser heating, the beam intensity was kept low.

III. RESULTS AND DISCUSSION

The focus of nanoindentation experiments was to observe the material's response to indentation under various loading conditions with a particular attention to the effect of cyclic loading. In case of nanoindentation, the conditions for phase transformation can be achieved even at a very low load because the contact area is small and the pressure is sufficiently high. Here we provide analysis of load-displacement curves based on information on indentation-induced phase transformations obtained from Raman microanalysis.

A. Gallium arsenide

A typical load versus displacement plot of nanoindentation (Fig. 1) consists of two parts, loading and unloading. The unloading curve does not overlap with the loading curve due to the residual irreversible deformation, which results in a nonzero displacement when the load is completely removed at the end of the experiment. If material underneath the indenter transforms into a new phase when certain stress conditions are met, changes in the slope of the loading/unloading curve or discontinuities in the loading/unloading curves are expected. In cyclic nanoindentation, additionally, any displacement of the reloading part of the curve relative to the unloading curve of the previous loading cycle, hysteresis, etc., must be considered as possible signs of phase transformation.

The slope of the loading curve of GaAs in each cycle [Fig. 1(a)] almost coincides with the slope of the unloading curve of the previous cycle. The unloading curve and elastic portion of the reloading curve do overlap. The elastic portion of reloading curve during interrupted tests has the same slope [Fig. 1(c)]. As shown earlier,[12] the slope of the elastic portion of reloading curves does not depend on the test conditions or depth of the indent and is a characteristic of the material. This means that the mechanical properties of the material in the indent do not change with reloading. There is no or a very small hysteresis, no pop-out, and no elbow.

GaAs has been predicted to transform to orthorhombic *Cmcm*[13] phase at about 12.5 GPa, and complete transformation was achieved in pressure cell experiments at 17.5 GPa.[14] These values are significantly higher than the room-temperature hardness of GaAs (Table I). A SEM micrograph of a typical nanoindentation in GaAs

TABLE I. Semiconductors under study.

Semiconductor type	Material	Structure	Band gap[32] (eV)	Microhardness[33] (GPa)	First metallic phase	Transition pressure (GPa)
IV	Si	Diamond cubic	1.12	12–14	β–Sn	12
IV	Ge	Diamond cubic	0.67	10	β–Sn	10.6
III–V	GaAs	Zincblende	1.4	6	*Cmcm*	12.5

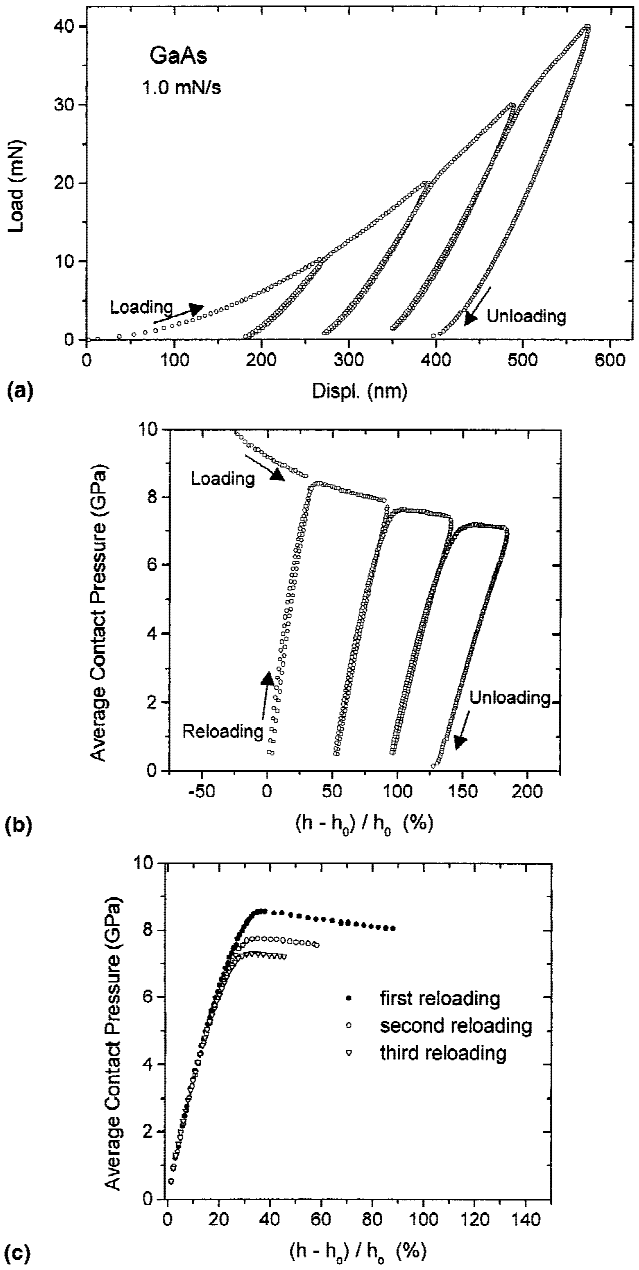

FIG. 1. (a) Load displacement curves, (b) ACP versus relative depth curves, and (c) reloading parts of the ACP depth curves for GaAs obtained at 1 mN/s.

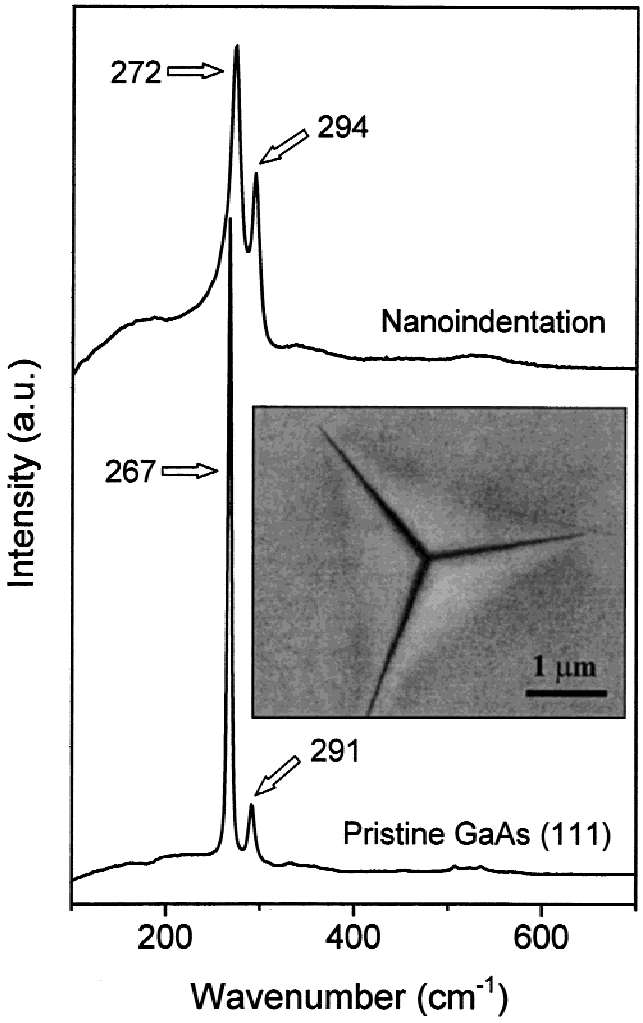

FIG. 2. SEM micrograph of a Berkovich indentation on GaAs obtained at the load of 70 mN and Raman spectra of GaAs on the wafer surface and in a nanoindentation. Changes in Raman spectra after indentation (broadening and shift of Raman bands) do not provide sufficient evidence of a phase transformation.

(Fig. 2) does not have any features that could be assigned to pressure-induced metallization. It is typical for indentations in ductile metals.

Raman analysis of nanoindentations on GaAs wafers (Fig. 2) demonstrated only a decrease in intensity of the transverse optical phonon band (267 cm^{-1}) relative to the intensity of longitudinal optical phonon band (291 cm^{-1}), band broadening due to residual deformation, and a shift to higher wavenumbers due to residual compressive stress. Increased background intensity between 100 cm^{-1} and 300 cm^{-1} may be ascribed to partial amorphization or disorder of GaAs structure. This suggests significant lattice damage after indentation experiments, which may be explained by extreme deformation during loading. Because the metallization pressure of GaAs is much higher than its hardness (Table I), a significant deformation hardening may be required, unless the transformation is driven by deformation rather than stress, as suggested by Gilman.[15]

The above analysis implies that no phase transformation occurs in GaAs under the indenter. The indentation behavior of GaAs is controlled by dislocation gliding similar to that of metals. However, at sufficiently low temperatures, the hardness of GaAs may be high enough to start a pressure-induced phase transformation during

indentation.[7] In support of this point, scratch experiments in liquid nitrogen at −196 °C demonstrated metallization-induced ductility of GaAs.[16]

B. Silicon

When the pristine cubic diamond phase of silicon (Si-I) is compressed to 10–13 GPa, it transforms to a metallic β–Sn structure (Si-II).[17,18] This transformation is accompanied by a 22% volume reduction. During pressure release from the metallic phase, there is a transformation to the semiconducting phases Si-XII (*r8* structure) and Si-III (*bc8* structure), metastable at ambient conditions.[18] The formation of metallic Si is possible in indentation experiments because the fine point of the indenter renders nonhydrostatic stresses of a very high magnitude controlled by the hardness of the indented material.[1,4,19] The pressures for the onset of the Si-I to Si-II transformation as well as the Si-II to Si-III transformation have been identified using spherical indenters of various radii.[20,21] This research confirmed that the phase transformation under indenter occurred when it reached about the same phase-transforming pressures observed in diamond anvils and hydrostatic pressure cell devices.[20] Moreover, high shear stress in indentation compared to high-pressure cells can favor phase transformations.[15,22]

Typical load-displacement curves for cyclic indentation (interrupted test) on Si are shown in Fig. 3(a). In contrast to GaAs, wide hysteresis loops are observed for Si, with their shape changing from cycle to cycle. The hysteresis loop is caused by a considerable change in volume during phase transformation and by the fact that the pressures of the direct and inverse phase transformations are different. In general, three different types of loops can be distinguished.

Loops of type 1 produced at low (10 mN) loads (Fig. 3) exhibit variations in the unloading curve slope at a pressure below 5 GPa [the AB region of the first unloading curve, Fig. 3(b)]. In reloading of the indent, a shoulder is observed on the loading curve at 12 GPa [the CD region, Fig. 3(b)]. With the pressure decrease, metallic silicon can transform either to the amorphous state or to crystalline phases Si-XII and Si-III. This phase transformation is reversible.[23] Therefore, the phase transformation to metallic phase is observed again at about 12 GPa during reloading [CD region in Fig. 3(b)].

Loops of type 2 type are typically observed at higher (>30 mN) loads (Fig. 3) and are characterized by a pop-out [EF in Fig. 3(b)]. After formation of discontinuity, the slope of the unloading curve increases.

Loops of type 3 are typical for the third or fourth cycle (Fig. 3), but sometimes are observed in the second cycle as well. They feature a hump (yield-point phenomenon), which is marked with a double-line arrow in Fig. 3(a). The ductility becomes more pronounced after several loading cycles and leads to behavior similar to Haasen–Kelly effect[24] that was observed for several metals due to yielding of the deformed surface layer earlier as compared to the bulk material. Such hump was observed during interrupted tensile tests on silicon at 850 °C.[25] At this temperature, the yield stress is much less than the metallization pressure and the discontinuity (step) is absent. We observed such humps after several cycles at room temperature. If a hump formation takes place, then

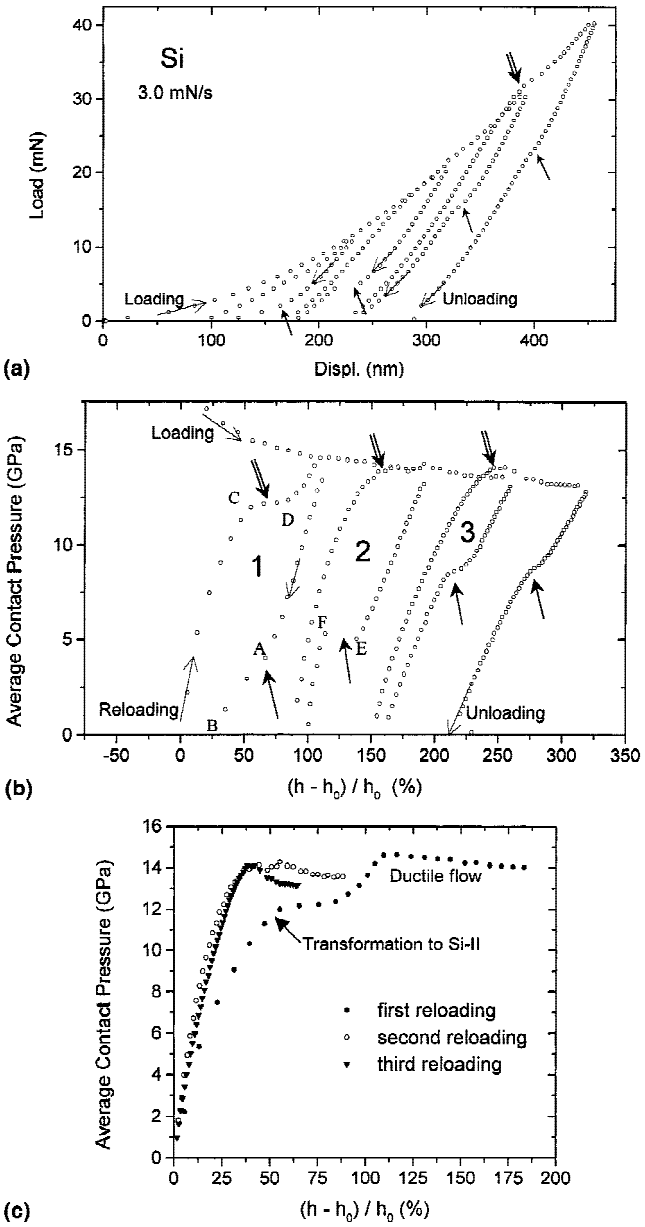

FIG. 3. (a) Representative load displacement and (b) ACP versus relative depth curves of cyclic indentation on Si obtained at the loading rate of 3 mN/s. (c) Reloading parts of the curves for three cycles. Double-line arrows mark formation of Si-II and single-line arrows mark the reverse transformation of Si-II and the loading–unloading direction.

the step at 12 GPa is absent. This can result from plasticity either in amorphous Si or in metallic Si remaining in indents due to a sluggish reverse transformation and high residual stresses (constrain of nontransformed Si around the indentation). Extrusion of the ductile metallic silicon from the indent, which was observed by SEM,[4] can also explain such behavior. However, it is important to note that extrusion of a metallic phase not necessarily accompanies phase transformations in Si. We observed many nanoidentations that did not show extrusions, but contained metastable phases of Si (Fig. 4). In cyclic indentation, the slope of the first (elastic) portion of the reloading curve increases after each loading cycle [Fig. 3(c)]. For silicon, the slope increases only when the transition from type-1 loop to type 2 takes place. Reloading curves for type-2 and type-3 loops have the same slope [Fig. 3(c)]. It means that the reloading of the same phase occurs in loops 2 and 3. In a material that does not show an indentation-induced phase transformation, the slope does not change [Fig. 1(c)].

It is important to note that the phase transformation from Si-I to Si-II does not produce any step on the loading curve in the first indentation cycle. This is due to the fact that even under the lowest loads, a pressure developed under the sharp Berkovich indenter is high enough for the silicon transition into the metallic state; thus the Si-I to Si-II transformation occurs during the whole loading part of the first cycle. In penetration of the Berkovich indenter into silicon, attempts to observe transition of silicon Si-I to metallic state Si-II have not met success.[26,27] However, Si-I to Si-II phase transition was directly observed in experiments using a spherical indenter.[20,21] In the case of a spherical indenter, the pressure needed for silicon transition to the metallic state develops at higher loads as compared to that in case of a sharp Berkovich indenter. It results in a change of a loading curve slope. In reloading test, the Si-I was absent in the indent and the step formation at 12 GPa pressure [Fig. 3(b)] is caused by transformation of metastable silicon phases to Si-II.

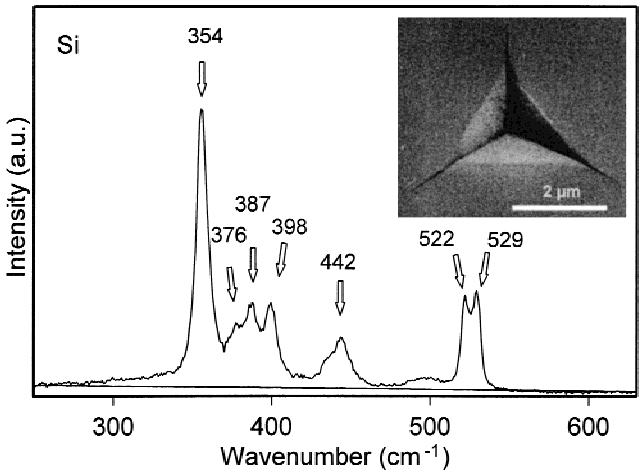

FIG. 4. SEM micrograph of a Berkovich indentation on Si produced with the load of 70 mN at the loading rate of 3 mN/s and a Raman spectrum from the center of the indent. The formation of metastable phases is clearly indicated by additional Raman bands.

Signs of phase transformation during unloading may be detected in various forms depending on the loading condition. In the case of silicon, the volume change during the phase transformation from Si-II to Si-XII or Si-III is more than 10%. This allows detecting the phase transformation as an abrupt discontinuity in the unloading curves. The pop-out behavior in silicon had been studied with respect to the crystalline orientation, and it was concluded that it varied statistically without any noticeable trend related with orientations.[8] In our experiments, Si was consistent in displaying the pop-out effects (Fig. 3), which can be explained by the reverse phase transformation from a metallic phase. Our Raman analysis suggests that this pop-out is caused by transformation of Si-II to Si-XII. Depending on the loading rate and the cycle number, either pop-out or a gradual volume change was observed (Fig. 3). The pressure of the reverse transformation varies significantly from experiment to experiment and generally increases with each cycle until it reaches about 8 GPa. Probably this happens due to the decreasing constraint of pristine Si and presence of seeds of new phases after several loading cycles. Formation of cracks around the indent after cyclic loading can also result in relief of residual stresses in Si and earlier reverse transformation of metallic silicon. Even when the phase transformation occurs, its route depends strongly on the loading conditions, particularly on the unloading rate. As a microindentation study showed, only amorphous Si was formed after very fast unloading, whereas slow unloading produced a mixture of Si-III and Si-XII, with an increasing content of Si-III at very slow unloading.[3]

It is necessary to discuss when and how the high-pressure Si-XII can transform to Si-III, which is stable at ambient pressure. This transformation is expected to happen below 2–3 GPa.[23] However, as can be seen from the shift of the Raman band of Si-I (520.8 cm^{-1} in unstressed state) in Fig. 4, residual stress in Si-I surrounding nanoindentations exceeds 2 GPa and therefore Si-XII is the primary phase in nanoindentations. Taking into account the fact that Si-III and Si-XII were found to coexist in indents, this transformation can be sluggish and it may be difficult to determine the transformation point on the nanoindentation curve. On the other hand, a very slight slope change is sometimes noticeable at this pressure (e.g., third loop in Fig. 3). In addition, the points of the beginning of the reloading curve and the end of the unloading curve do not coincide. The difference is particularly noticeable for the first cycle at high loading rates. These features of the indentation curves may be assigned

to formation of Si-III at low pressures, primarily after 95% unloading. In situ Raman spectroscopy should help to clarify this issue.

C. Germanium

Ge has been much less studied than Si. Hainsworth *et al.*[8] did not find any elbows or pop-outs on unloading curves. However, TEM and conductivity studies,[1] along with our Raman spectroscopy investigations of microindentations,[16] suggest metallization of Ge in indentation. The only feature discussed in the literature[5] was the formation of small steps (pop-ins) on the loading part of the load displacement curve (Fig. 5). These were ascribed to microcracking in the indentation or dislocation plasticity.[8]

The transformation behavior of Ge can be seen as similar to that of Si. In the case of Ge, there is a transition to the metallic β–Sn (Ge-II) structure at 10.6 GPa.[5,28,29] This transition is shear sensitive; i.e., the transition pressure can be reduced to 8 GPa in presence of additional shear stress. There are also several metastable phases, known from experiments in high-pressure cells,[30] which form during unloading from the metallic state. There exists the *hd* phase (Ge-V) and a simple tetragonal phase (*st12* or Ge-III). By fast pressure release, the *bc8* (Ge-IV) phase may be produced. It subsequently transforms to *hd* structure within a few hours.[28] Our previous Raman studies on Ge showed that there are several phases within Ge microindentations.[31] According to the high-pressure cell experiments, these phases are formed via the metallic β–Sn phase.

Our nanoindentation experiments demonstrated hysteresis loops (Figs. 5 and 6) that are very different from those observed on polymers or metals. The loops in metals and most of the semiconductors are very narrow. The loops in Ge are broad as for visco-elastic polymers, but the width did not decrease with decreasing loading rate, as it happens in visco-elastic materials.[11] The shape of the loop was also different from that in polymers. It is broad in the upper part and becomes narrow in the lower part. Broad asymmetric loops have been only published for Si, which as we know shows a phase transformation upon indentation. This shape of hysteresis curves should be ascribed to a phase transformation in Ge.

As noticed before,[5,8] unloading curves of Ge are fairly featureless [Fig. 5(a)]. However, replotting these curves as ACP versus indentation depth [Fig. 5(b)] revealed a clear elbow on the unloading curve, similar to that observed in Si [Fig. 3(b)]. Thus, a reverse phase transformation from metallic Ge occurs during unloading. It is less pronounced than that in Si and begins at a higher pressure, and not always in the first loading cycle. Thus, some deformation hardening may be required to drive metallization in Ge. This is in agreement with the nanoindentation data. Only rarely a kink could be clearly seen

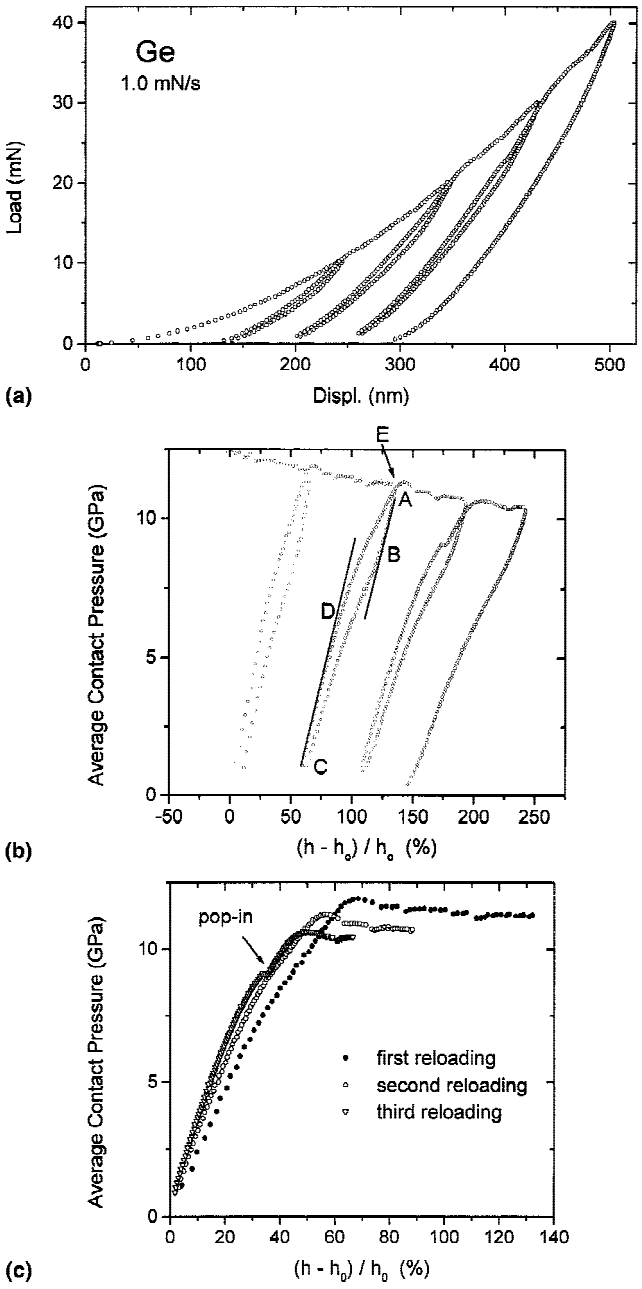

FIG. 5. (a) Representative load displacement, (b) ACP versus relative depth, and (c) reloading parts of the ACP depth curves of cyclic indentation for Ge obtained at the loading rate of 1 mN/s.

on load-displacement curves of Ge (Fig. 6) obtained at a high loading rate. These experiments produced noticeable amounts of amorphous Ge and suggest metallization of Ge under the indenter. Thus, Ge shows both metallization and plastic deformation in the indentation. Depending on the loading conditions, one or another process can dominate.

On the elastic part of the loading curve, a change in the slope is observed at about 7–8 GPa [point D in Fig. 5(b)]. The slope of the elastic part of the loading curve changed

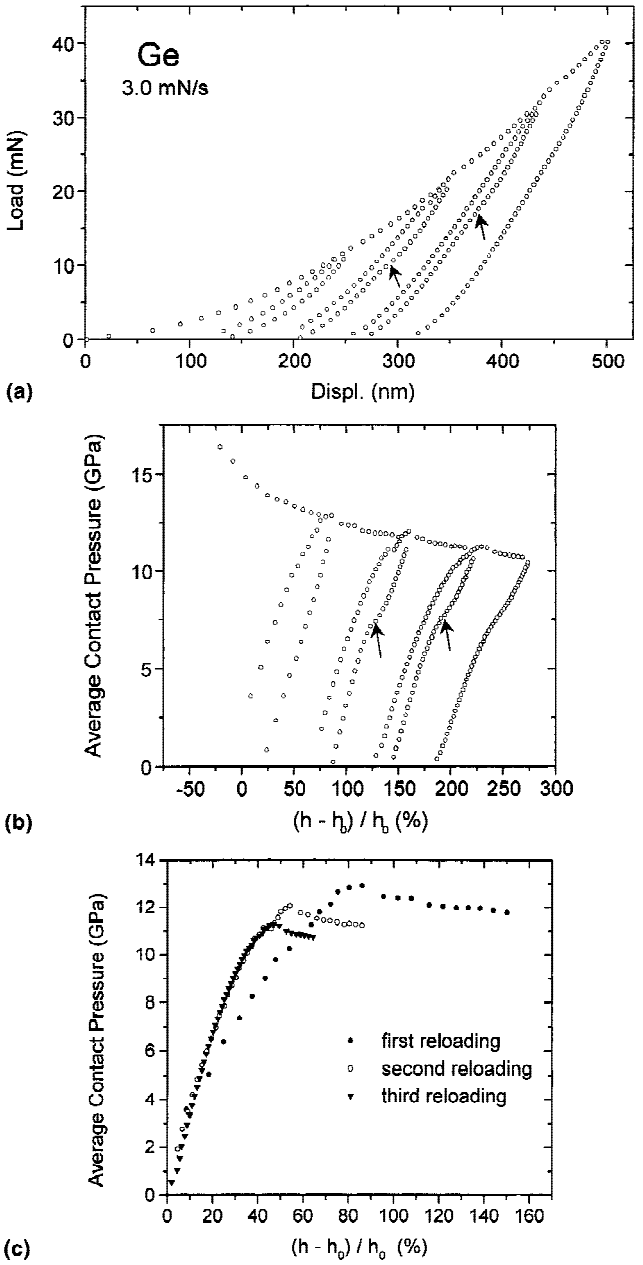

FIG. 6. (a) Load displacement curves, (b) ACP versus relative depth, and (c) reloading parts of the ACP versus depth curves for Ge obtained at the loading rate of 3 mN/s.

(increased) with each loading cycle [Fig. 5(c)]. It means that the elastic properties of Ge in the indentation change (decrease) due to pressure-induced phase transformation. Again, this change can be better seen when plotted as pressure versus depth [Fig. 6(b)]. Behavior similar to Haasen–Kelly effect has been also observed for Ge [point E in Fig. 5(b)]. It was more strongly pronounced in the first loading cycle and was becoming weaker after each loading.

Raman analysis of Ge wafers [Fig. 7(a)] demonstrated only a weak peak at about 295 cm^{-1} that can be assigned to *hd* phase formed by twinning of Ge-I, and a strongly shifted Ge-I band due to residual compressive stress in most indentations. This behavior, along with a pop-in on some of the loading curves, suggests the possibility of plastic deformation of Ge in the indent without or with a minor contribution from the pressure-induced metallization. However, in some of the indents, particularly the ones produced at a high loading rate, amorphous Ge (Raman band at 271–272 cm^{-1}) and traces of metastable phases (bands at 200, 225, and 245 cm^{-1}) were found [Fig. 7(b)]. SEM micrographs of the indents in Ge (Fig. 7) have features of both GaAs and Si. There is a significant elastic recovery resulting in the residual deformation primarily along edges of the pyramid, and there is material squeezed out of the indent, confirming the metallization of Ge and formation of a ductile metallic phase under the indenter.

The nanoindentation behavior of Ge can be explained as follows. In the AB range [Fig. 5(b)] unloading of metallic phase occurs. In point B, metallic phase begins to transform into amorphous Ge with a volume increase, leading to a faster decrease of the indent depth with decreasing pressure. The reverse transformation is completed in point C. The next loading cycle starts with loading the metastable phase or amorphous Ge in the indent (CD range). At about 8 GPa, Ge transforms into metallic phase and the deformation rate increases due to decreasing volume of the material and a higher plasticity of the metallic phase. In some cases, steps in the DE range were observed. We assume that these steps can be a result of extrusion of the ductile metallic phase that was observed for Si and Ge and acted as evidence of their metallization in indentation.

It is important to explain the difference in the results that we obtained and those published by other researchers.[6,8] In previous experiments, Ge was loaded with the same load in each cycle. The amount of amorphous Ge in indentation increased with each cycle and the loop width decreased. In our experiments, the load increased in each cycle, and pristine Ge was involved in the experiment.

IV. CONCLUSIONS

It has been demonstrated that Raman microspectroscopy can be used to study phase transformation in nanoindentations even if the indent size is smaller than the laser spot size. Raman analysis allows for assignment of certain features of load-displacement curves to phase transformations under the indenter.

Phase transformation of Si-I to Si-II under indenter results in a yield step and/or slope change of the upper part of the loading curve. A pop-out, kink, or elbow have

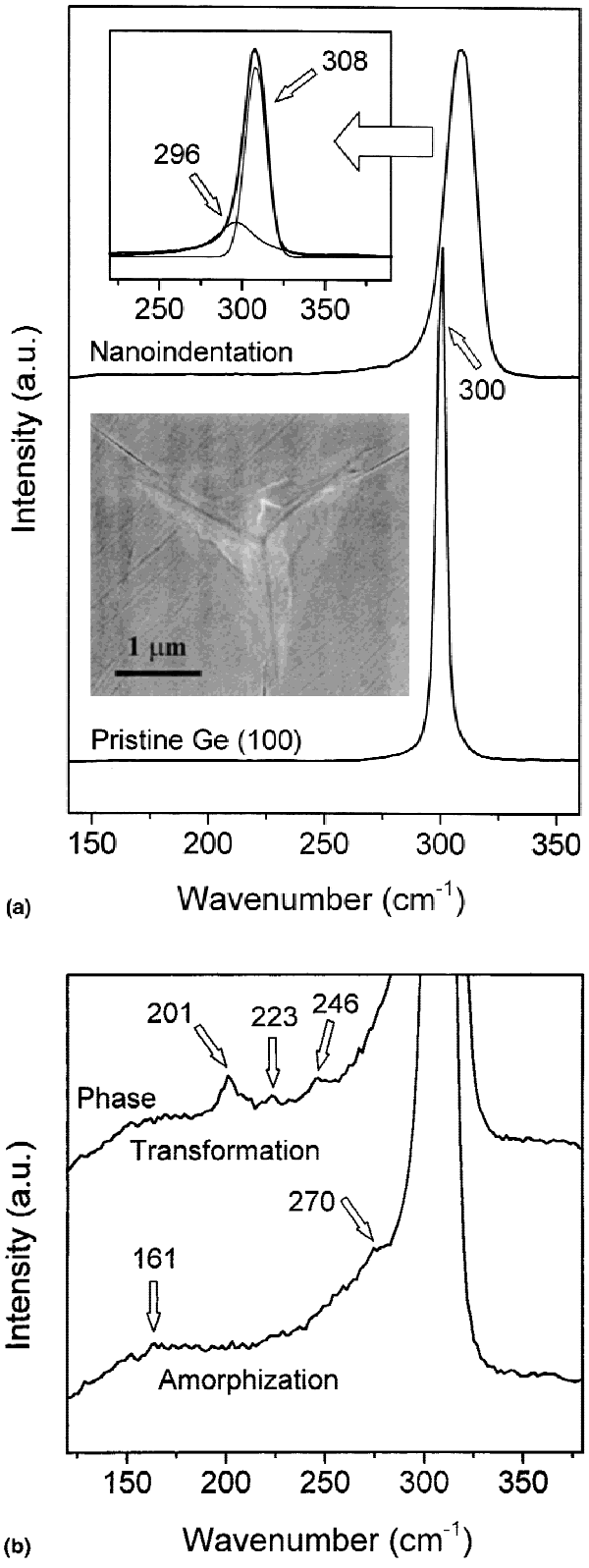

FIG. 7. (a) SEM micrograph of a Berkovich indentation on Ge obtained at the load of 70 mN and typical Raman spectra of Ge on a wafer surface and in a nanoindentation and (b) metastable and amorphous Ge phases found in some nanoindentations produced at high loading rates.

been always observed on the unloading part of the curve and assigned to reverse transformation of metallic Si-II to Si-XII or amorphous silicon.

Similar to Si, germanium shows metallization under load, but the role of plastic deformation becomes more significant. The reverse transformation in Ge is less pronounced resulting in a kink rather than discontinuity on the unloading curve. Other features of load-displacement curves are similar to that of Si.

The nanoindentation experiments on GaAs do not show any signs of pressure-induced metallization at room temperature. This is in agreement with Raman data.

Nanoindentation experiments can supply reliable information on pressure-induced phase transformations in semiconductors if they cause change in volume or mechanical properties of the material in indentation. The formation of the ductile metallic phase results in a yield step and/or slope change of the upper part of the loading curve. Reverse phase transformation of metallic phases results either in a pop-out or in a slope change (elbow) of the unloading part of the load-displacement curve. Broad and asymmetric hysteresis loops in cyclic indentation, as well as a discontinuity in unloading/reloading curves, can be used for confirmation of a phase transformation in indentation.

Depth-sensing indentation can be used for measurement of phase transformation pressures. Metallization pressure can be determined as the average contact pressure (Meyer's hardness) for the yield point on the loading curve. The pressure of the reverse transformation of the metallic phase can be measured from pop-out or elbow on the unloading part of the diagram. For materials with phase transformations less pronounced than in Si, replotting of the load-displacement curves as ACP versus relative depth $(h - h_o)/h_o$ may be required to determine the transformation pressures and/or improve the accuracy of measurements.

ACKNOWLEDGMENTS

The research at the University of Illinois at Chicago was supported by the National Science Foundation, Grant No. DMI-9813257. The research at the University of Tübingen was supported by the German Research Society (DFG, Ni-299/6).

REFERENCES

1. D.R. Clarke, M.C. Kroll, P.D. Kirchner, R.F. Cook, and B.J. Hockey, Phys. Rev. Lett. **60,** 2156 (1988).
2. Y.G. Gogotsi, A. Kailer, and K.G. Nickel, Materials Research Innovations **1,** 3 (1997).
3. A. Kailer, Y.G. Gogotsi, and K.G. Nickel, J. Appl. Phys. **81,** 3057 (1997).
4. G.M. Pharr, W.C. Oliver, and D.S. Harding, J. Mater. Res. **6,** 1129 (1991).

5. G.M. Pharr, W.C. Oliver, R.F. Cook, P.D. Kirchner, M.C. Kroll, T.R. Dinger, and D.R. Clarke, J. Mater. Res. **7,** 961 (1992).
6. G.M. Pharr, W.C. Oliver, and D.R. Clarke, J. Electron. Mater. **19,** 881 (1990).
7. J.J. Gilman, J. Mater. Res. **7,** 535 (1992).
8. S.V. Hainsworth, A.J. Whitehead, and T.F. Page, in *Plastic Deformation of Ceramics*, edited by R.C. Bradt, C.A. Brookes, and J.L. Routbort (Plenum Press, New York, 1995), p. 173.
9. J.C. Morris and D.L. Callahan, in *Microstructure of Materials*, edited by K.M. Krishnan (San Francisco Press, San Francisco, 1992), p. 104.
10. D.L. Callahan and J.C. Morris, J. Mater. Res. **7,** 1614 (1992).
11. N.V. Novikov, S.N. Dub, Y.V. Milman, I.V. Gridneva, and S.I. Chugunova, Sverkhtverdye Materialy (Superhard Materials) **18,** 37 (1996).
12. S.N. Dub, in *Thin Films: Stresses and Mechanical Properties VII*, edited by R.C. Cammarata, M. Nastasi, E.P. Busso, and W.C. Oliwer (Mater. Res. Soc. Symp. Proc. **505,** Warrendale, PA, 1998), pp. 223–228.
13. M.I. McMahon and R.J. Nelmes, Phys. Status Solidi B **198,** 389 (1996).
14. J.M. Besson, J.P. Itie, A. Polian, G. Weill, J.L. Masot, and J. Gonzalez, Phys. Rev. B **44,** 421 (1991).
15. J.J. Gilman, Czech J. Phys. **45,** 913 (1995).
16. Y. Gogotsi, M.S. Rosenberg, A. Kailer, and K.G. Nickel, in *Proceedings of the Workshop on Tribology Issues and Opportunities in MEMS*, edited by B. Bhushan (Kluwer, Dordrecht, The Netherlands, 1998), pp. 431–442.
17. R.J. Needs and A. Mujica, Phys. Rev. B **51,** 9652 (1995).
18. R.O. Piltz, J.R. Maclean, S.J. Clark, G.J. Ackland, P.D. Hatton, and J. Crain, Phys. Rev. B **52,** 4072 (1995).
19. I.V. Gridneva, Y.V. Milman, and V.I. Trefilov, Phys. Status Solidi A **9,** 177 (1972).
20. E.R. Weppelmann, J.S. Field, and M.V. Swain, J. Mater. Res. **8,** 830 (1993).
21. E.R. Weppelmann, J.S. Field, and M.V. Swain, J. Mater. Sci. **30,** 2455 (1995).
22. M.C. Gupta and A.L. Ruoff, J. Appl. Phys. **51,** 1072 (1980).
23. J. Crain, G.J. Ackland, J.R. Maclean, R.O. Piltz, P.D. Hatton, and G.S. Pawley, Phys. Rev. B **50,** 13043 (1994).
24. P. Haasen and A. Kelly, Acta Metall. Mater. **5,** 192 (1957).
25. V.P. Alekhin, *Physica Prochnosti i Plastichnosti Poverkhnostnykh Sloev Materialov* (Nauka, Moscow, 1983).
26. B. Bhushan, A.V. Kulkarni, W. Bonin, and J.T. Wyrobek, Philos. Mag. A **74,** 1117 (1996).
27. T.F. Page, W.C. Oliver, and C.J. McHargue, J. Mater. Res. **7,** 450 (1992).
28. R.J. Nelmes, M.I. McMahon, N.G. Wright, D.R. Allan, and J.S. Loveday, Phys. Rev. B **48,** 9883 (1993).
29. C.S. Menoni, J.Z. Hu, and I.L. Spain, Phys. Rev. B **34,** 362 (1986).
30. C.H. Bates, F. Dachille, and R. Roy, Science **147,** 860 (1965).
31. A. Kailer, Y.G. Gogotsi, and K.G. Nickel, in *High Pressure Materials Research*, edited by R.M. Wentzcovitch, R.J. Hemley, W.J. Nellis, and P.Y. Yu (Mater. Res. Soc. Symp. Proc. **499,** Warrendale, PA, 1998), pp. 225–230.
32. N.W. Ashcroft and N.D. Mermin, *Solid State Physics* (Saunders College Publishing, Philadelphia, PA, 1976).
33. A.B. Chen, A. Sher, and W.T. Yost, in *The Mechanical Properties of Semiconductors*, edited by K.T. Faber and K. Malloy (Academic Press, London, 1992), Vol. 37, p. 68.